Residence time distribution in single big industrial flotation cells

J. Yianatos, L. Bergh and K. Tello
Chemical engineer, chemical engineer and metallurgical engineer, respectively, Department of Chemical Engineering, Santa María University, Valparaíso, Chile

F. Díaz
Chemical engineer, Nuclear Applications Department, Chilean Commission of Nuclear Energy, Santiago, Chile

A. Villanueva
Metallurgical engineer, Department of Metallurgical Engineering, División El Teniente, Codelco-Chile

Abstract
The collection zone residence time distribution (RTD) of mechanical self-aerated flotation cells was characterized for liquid and solid per size class (-45 μm, +45-150 μm and +150 μm). It was found that a single large industrial cell with a volume of 130 to 250 m^3, now used in plant operations, can be well represented by an LTST (large and small tank-in-series) model plus dead time. From a scale-up point of view, results showed a similar mixing behavior for industrial cells ranging from 130 to 250 m^3. Also, single mechanical cells showed a similar mixing pattern (RTD) when compared to large pneumatic flotation columns. It was confirmed that for practical purposes, the mixing condition in a flotation bank of three or more cells in series can be well described by the classical N tanks-in-series model.

Key words: Modeling, Flotation, Flotation machines, Residence time distribution

Introduction
Flotation cell requirements. Flotation cells need to accomplish functions such as air bubble dispersion and solid suspension, and they must provide the best conditions for bubble-particle collision and aggregate formation. For this reason, cells are typically provided with mechanical agitation systems that generate well-mixed conditions for the pulp and air bubbles. In an industrial, continuous mechanical cell, however, the mixing condition prevents some particles from having the same opportunity to be collected because a significant fraction of the particles spend a very short time in the cell (in a well-mixed condition, almost 40% of the particles stay in the cell for less than half of the mean residence time).

Flotation bank arrangement. Assuming the flotation cells are perfectly mixed, time scale-up factors of four and seven can be predicted when comparing a single continuous industrial cell with a laboratory batch process at 90% and 95% recovery, respectively. These factors are due only to the change of the mixing condition, considering the same rate constant (Arbiter, 2000). For this reason, industrial cells are typically arranged in banks consisting of a series of cells. In practice, using an arrangement of six or more cells in series, the time scale-up factor can be decreased to 1.2 for the same rate constant. Thus, the mixing effect became less significant compared to typical time scale-up factors for flotation plants, around 2.2 to 4.2, where the main effect was related to the change in rate constant (Yianatos et al., 2005a).

Flotation cells characterization. Figure 1 shows a self-induced air mechanical flotation cell that includes a central draft tube to allow pulp circulation and contact with air bubbles generated when the induced air and pulp circulate through the rotor, which is located in the upper part of the cell below the pulp-froth interface. The rotor is also surrounded by a disperser-stator and a disperser hood to provide a quiescent pulp-bubble separation region near the pulp-froth interface. The cell design also includes a froth crowder, with the shape of an inverted cone, to increase the froth velocity by reducing the flow area, thus improving the froth transport and mineral discharge into the concentrate launders. The cell is also provided with vertical baffles and radial launders.

The perfect mixing condition of the pulp in flotation cells is a common assumption for process modeling (Jowett, 1961; Woodburn and Loveday, 1965; Niemi, 1966; Har-

Paper number MMP-07-007. Original manuscript submitted March 2007 and accepted for publication April 2007. Discussion of this peer-reviewed and approved paper is invited and must be submitted to SME Publications Dept. prior to Aug. 31, 2008.

ris, 1978; Mehrotra and Saxena, 1983; Burgess, 1997; King, 2001; Deglon, 2003). However, observations and discussions about the non-perfect mixing behavior in flotation cells has been reported for many years (Huber-Panu et al., 1976; Harris, 1978; Mavros, 1991). Thus, a more realistic approach to describe the mixing condition in the pulp of industrial cells is the use of the actual RTD function (Niemi, 1995; Polat and Chander, 2000).

Data from industrial RTD measurements in single large size cells is scarce. Burgess (1997) showed that the RTD of a 100-m^3 flotation cell provided with forced air was close to well mixed. More recently, Lelinski et al. (2002) reported on a comparison between the RTD of three flotation cells, 148 to 160 m^3, tested in parallel. Here, it was observed that cells operating with forced air and with the rotor located near the bottom also showed a RTD close to well-mixed, while the self-aerated cells, as shown in Fig. 1, showed a more significant deviation from perfect mixing.

Industrial banks of large size cells have been characterized as perfect mixers in series (Cortés et al., 1995, Perez-Correa et al., 1998; Arbiter, 2000). Also, by using radioactive tracer tests it was shown that the RTD of flotation banks consisting of four, eight and nine cells can be well represented by a simple model consisting of the same number of cells, operating like perfect mixers in series, plus a dead time (Yianatos et al., 2001; Yianatos et al., 2005b).

From a metallurgical point of view there is no significant effect on estimating the overall bank recovery using the perfect mixers approach to describe the RTD of the bank. However, to identify the true flotation rate constant of the collection zone, particularly in large-size flotation cells, it is relevant to know the actual mixing conditions of the minerals, liquid and air in the cell. The knowledge of the true rate constant of the collection zone is possible, provided an independent measurement of the froth zone recovery is available (van Deventer et al., 2001; Alexander et al., 2003; Seaman et al., 2004). Thus, the flotation rate constant can be properly characterized in terms of relevant factors such as mineral properties (grade, liberation, size) and operating conditions (reagents, pulp density, airflow rate, bubble size, bubble surface area flux) in the plant.

Flotation bank: A distributed flotation system. The flotation bank is a distributed multistage system where the flow rate, solids percent, mineral and pulp properties change cell by cell. Also, the operating conditions, such as airflow rate, pulp level and eventually reagent addition, can be manipulated independently for each cell or cell arrangement.

The most common approach for flotation bank modeling is to perform an overall mass balance around the bank and to model the whole system using a classical kinetic model (Perez-Correa et al., 1998; Yianatos et al., 2000, 2005a).

The flotation bank models commonly used for design or scale-up purposes only consider a single rate constant and a mean residence time, which are the same for all cells. Thus, the implicit assumption is that in a flotation bank, all the cells operate under the same condition, and using an overall rate constant and dead time hinders the actual differences in time and operation. This approach can be useful in terms of circuit design. However, it is quite limited regarding the analysis, control and optimization of the flotation bank operation.

The key question is how to set the manipulated variables along the flotation bank. This problem becomes more relevant when using large-size flotation cells, which deviate more from perfect mixing conditions, with the potential of using shorter banks, i.e., four to six cells per bank (Bourke, 2002).

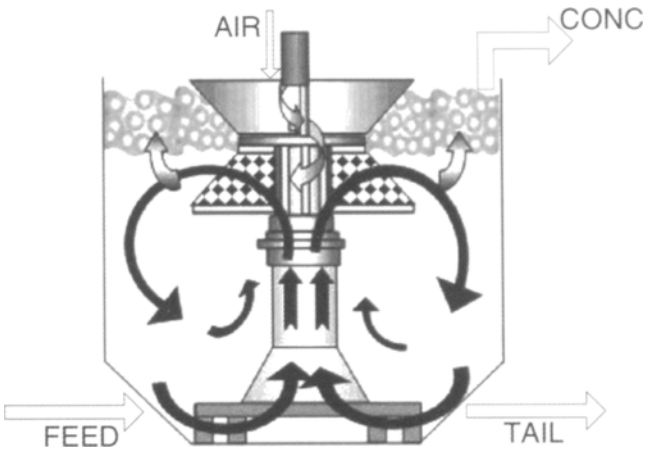

Figure 1 — Self-induced air mechanical flotation cell.

To identify the optimal bank operating condition, a new approach is being considered where the operation of a single cell will be characterized independently in terms of collection zone rate constants and froth recovery. In both zones, the key parameters will be linked with the manipulated variables. For this purpose, the actual mixing condition in a single flotation cell must be characterized. With this aim, the present paper describes a study on the residence-time distribution in large-size industrial flotation cells (130 m^3) as a first step in building up a practical metallurgical model capable to simulate the actual distributed process.

Modeling

Model selection. To characterize the metallurgical behavior of mechanical cells arranged in banks, the residence time distribution (RTD) has been typically represented by a model of N perfect mixers in series (Mavros, 1992, Cortés et al., 1995; Yianatos et al., 2001, 2005b),

$$E(t) = \frac{(t-L)^{N-1} \exp\left[-(t-L)\cdot N/\tau\right]}{(\tau/N)^N \cdot \Gamma(N)} \quad \text{for } t > L \qquad (1)$$

where

τ is the mean residence time,

L is the lag time and

$\Gamma(N)$ is the gamma function that replaces the factorial term $(N-1)!$ to account for the non-integer solutions of N.

Thus, the normalized distribution function, gamma model, can be obtained in terms of the dimensionless time θ from

$$E(\theta) = \frac{\theta^{N-1} N^N \exp(-\theta \cdot N)}{\Gamma(N)} \qquad (2)$$

where

$$\theta = (t-L)/\tau \qquad (3)$$

For a single cell, Eq. (2) reduces to the typical response of a perfect mixer. Thus, for $N = 1$

$$E(\theta) = \exp(-\theta) \qquad (4)$$

However, the new experimental evidence presented below confirms that the perfect mixing condition is not valid for single industrial flotation cells of large size, which are commonly used in most new installations. Thus, it is shown below that a better fit to the actual process data can be obtained using a simple

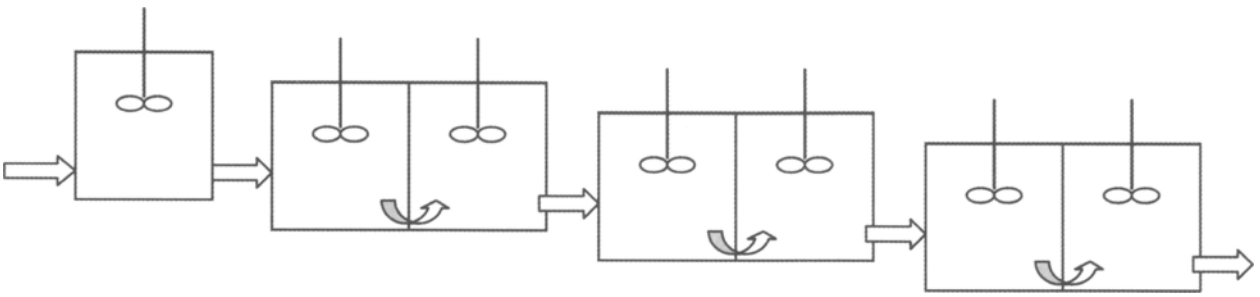

Figure 2 — Flotation cells bank consisting of seven cells in a 1-2-2-2 arrangement.

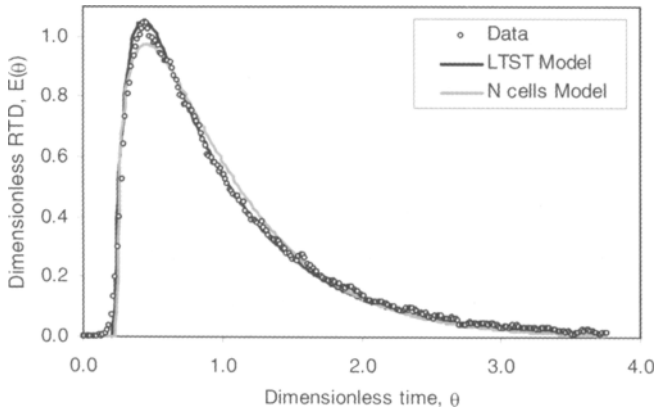

Figure 3 — Liquid RTD of the first cell in the rougher bank.

alternative LTST model to describe the RTD of a single large flotation cell. The LTST (large-and-small-tank-in-series) model consists of one large perfect mixer (residence time τ_L) and one small perfect mixer in series (residence time τ_S), plus a dead time τ_P. The analytical solution for this model is given by the following equation (see Appendix A for derivation)

$$E(t) = \frac{\exp\left[-(t-L)/\tau_s\right] - \exp\left[-(t-L)/\tau_L\right]}{\left(\tau_s - \tau_L\right)} \qquad (5)$$

where

L is the lag time.

Also, the normalized distribution function can be obtained in terms of the dimensionless time θ using

$$E(\theta) = \frac{\tau\left\{\exp\left[-(\theta\cdot\tau)/\tau_s\right] - \exp\left[-(\theta\cdot\tau)/\tau_L\right]\right\}}{\left(\tau_s - \tau_L\right)} \qquad (6)$$

where the overall mean residence time τ is

$$\tau = \tau_s + \tau_L + L \qquad (7)$$

Experimental procedure

Industrial flotation circuit. A comprehensive study was developed in the rougher flotation bank of the new concentrator at El Teniente Division, Codelco-Chile. The rougher circuit consists of four parallel lines, each one of seven cells in series, in a 1-2-2-2 arrangement, as shown in Fig. 2. Each self-aspirating Wemco cell has a nominal volume of 130 m^3.

Residence time distribution measurement in single cells. To study the hydrodynamic behavior of single cells, the radioactive tracer technique (Yianatos et al., 2005b) was used to measure the residence-time distribution of the liquid and solid in the cell. Thus, a radioactive tracer Br-82 solution in water was injected at the inlet of the first cell as the liquid tracer. Then, the response time of the radioactive tracer was measured on-line using a non-invasive sensor located directly in the discharge of the cell. Scintillating crystal sensors of NaI(Tl), 25.4 x 38.1 mm (1 x 1.5 in.), Saphymo Srat, were used for activity measurement. Also, nonfloatable mineral was used as the solid tracer. The solid tests considered the use of overall solid, as well as solid in three size classes: coarse (+150 μm), intermediate (-150+45 μm) and fine (-45 μm).

The individual performance of each cell along the bank was evaluated by a series of tests performed around each cell. For the first cell, the radioactive tracer was instantaneously injected through the feed box near the feed entrance of the cell, while for the other cells the tracer was injected directly inside the cell near the feed entrance. The RTD was measured online in the tailings stream of each cell. The procedure was repeated for the seven cells of the flotation bank.

Results

First cell RTD. Figure 3 shows the liquid response data. Here, the experimental data directly corresponds to the open loop impulse response of the first cell. Thus, an effective mean liquid residence time of 5.7 min was calculated for the first cell. This result shows that single self-aerated industrial flotation cells do not operate like a perfect mixer. The experimental RTD data observed in Fig. 3 was modeled using the N tank-in-series model Eq. (2), and the equivalent number of tanks-in-series was N = 1.38. Also, other models were tested, and the large and small tanks-in-series (LTST) model (Eq. (6)), gave the best fit while keeping a minimum number of parameters.

This kind of mixing pattern is related to the pumping effect of the rotor together with the shaft tube, Fig. 1, which provides the pulp circulation through the rotor as well as an effective contact between the pulp and bubbles generated by air dispersion in the rotor.

Figure 4 shows the experimental RTD data for the fine solid (-45 μm) in the first cell of the bank. Here, the LTST model (Eq. (6)) fit also showed the best agreement in describing the data trend along the response time. Similar results were found for the medium and coarse particles.

Bypass flow. Figure 5 shows the liquid RTD in Cell 3, where an abnormal operating condition because of bypass flow (short-circuiting) was observed, probably related to solid settling. A similar condition was also observed in Cell 4. Figure 5 also

Table 1 — Model parameters adjustment.

Parameters	Cell 3	Cell 4
τ_b, min	0.05	0.05
N	10	10
L	0.63	0.509
τ_S, min	0.559	0.365
τ_L, min	4.442	4.988
a, %	6.0	9.0
Error x 10^{-6}	9.5369	3.9315

shows the fitting of a RTD model, including bypass flow, derived to describe this kind of flow behavior. The model considers the split of the feed stream into a smaller feed fraction (a), representing the bypass flow (closer to a plug flow) and a larger feed fraction (1 - a), which represents the overall mixing condition in the cell (Bazin and Hodouin, 1988). Figure 6 shows the model diagram to describe the mixing in flotation cells including bypass.

The analytical solution of this model in the Laplace domain is given by

$$E(s) = a \cdot \frac{1}{\left(1+\tau_b s\right)^N} + (1-a) \cdot \frac{\exp(-Ls)}{\left(1+\tau_S s\right)(1+\tau_L s)} \qquad (8)$$

In this model, the bypass flow was represented by a series of N perfect mixers with equal residence time τ_b, and the mixing zone was represented by the LTST model plus dead time (see Eq. (A4) in Appendix A). The model includes a weighting factor (a) that represents the feed fraction bypassed inside the cell. Table 1 shows the model parameters obtained from the experimental data fit in Cells 3 and 4. Here, it was observed that Cell 3 had 6% bypass flow while Cell 4 had 9% bypass flow. The impact of these percentages of bypass flow was not significant in terms of mineral recovery. However, the prompt detection of this kind of problem prevents operating troubles in the long term because of solid sanding.

The short time delay (L) in Cells 3 and 4 corroborates that bypass flow exists, because these times are lower than the necessary time for pulp recirculation throughout the rotor, approximately 70 seconds (Larenas, 2006).

Comparison of the RTD of single cells in a flotation bank. Table 2 shows the comparison of LTST and N cells models

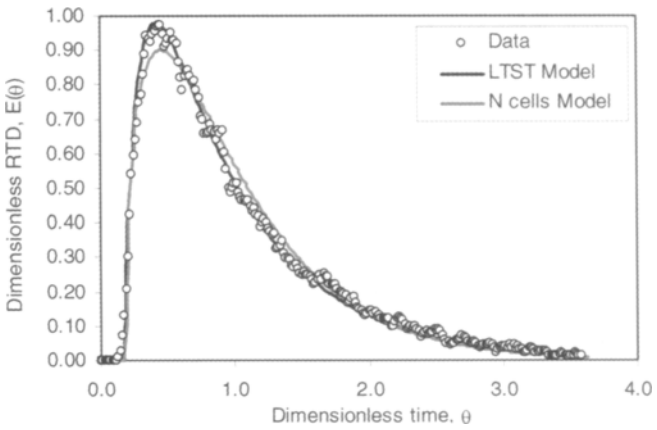

Figure 4 — Fine solid RTD of the first cell in the rougher bank.

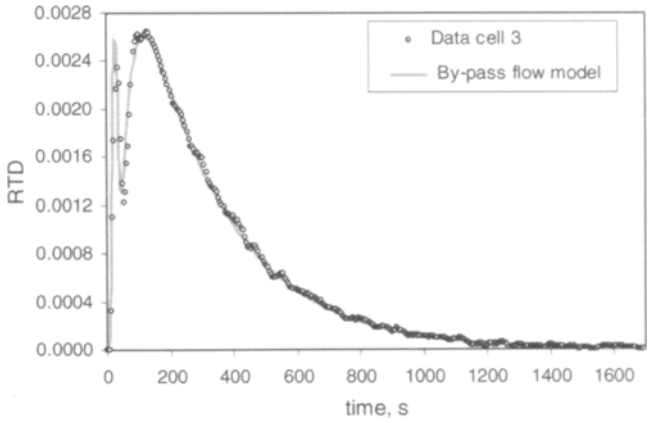

Figure 5 — Liquid RTD in Cell 3 showing bypass flow.

for Cells 1, 2, 5, 6 and 7, operating under normal conditions, in the rougher flotation bank. Also, the corresponding number N of equivalent tanks-in-series is presented. Modeling of Cells 3 and 4 was previously presented in Table 1.

It can be seen that the mixing condition in a single large size flotation cell is equivalent to 1.1 to 1.4 perfect mixers in series, plus dead time. Therefore, it was verified that single big cells do not perform as a perfect mixer. Also, it was observed

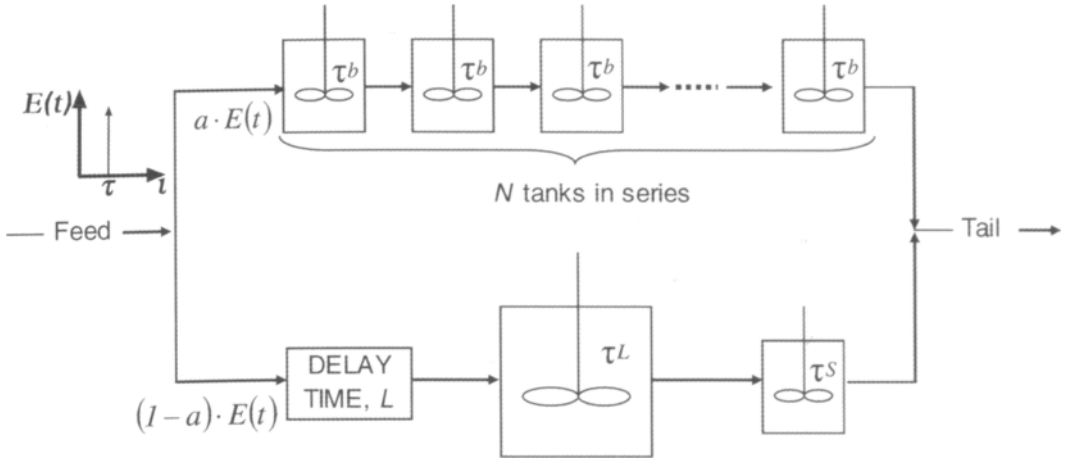

Figure 6 — Mixing model of cells with bypass flow.

Table 2 — Comparison of LTST vs. N tank-in-series model for a single cell.

Model	Parameter	1	2	5	6	7
N cells	N	1.38	1.07	1.26	1.13	1.14
	τ, min[1]	4.32	5.58	5.12	5.63	4.89
	L, min	1.40	1.17	0.74	0.92	0.92
	Error x 10^{-6}	2.0198	1.4491	2.3426	3.5398	2.1550
	τ_{total}, min	5.72	6.75	5.86	6.55	5.81
LTST	τ_S, min	0.572	0.133	0.442	0.225	0.217
	τ_L, min	4.097	5.188	5.068	5.690	4.959
	L, min	1.273	1.060	0.605	0.808	0.816
	Error x 10^{-6}	0.1423	1.2415	1.1845	2.0040	1.3488
	τ_{total}, min	5.942	6.381	6.115	6.723	5.992
Number of points:		1,285	1,230	1,525	1,330	1,300
Feed Solid Flow, tph:		2,030	2,470	2,450	2,380	2,500

[1] Mixing time for N cells.

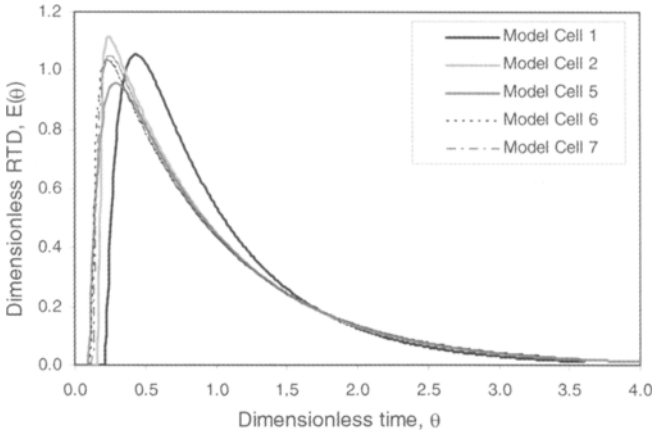

Figure 7 — Comparison of dimensionless liquid RTD for single cells in a bank.

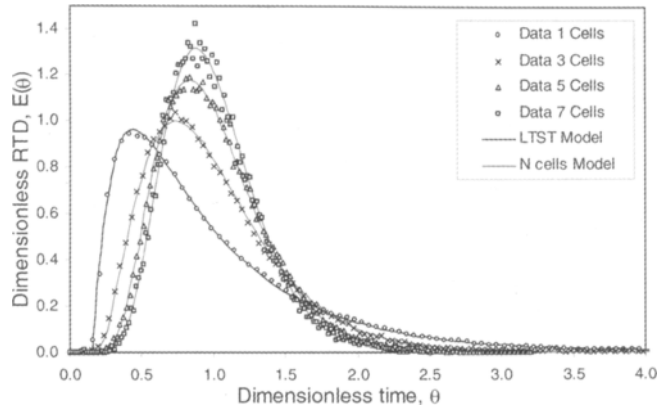

Figure 8 — RTD along the rougher flotation bank: 1, 3, 5 and 7 cells in series.

that the LTST model is better to represent the hydrodynamic behavior of single big cells.

Figure 7 shows the dimensionless comparison of the RTD of Cells 1, 2, 5, 6 and 7 of the flotation bank, represented by the LTST model (Eq. (6)), adjusted for each cell from experimental data. Here, models from Cells 2, 5, 6 and 7 show a consistent pattern with time delay of less than 70 seconds. This means that a fraction of tracer was removed from the cell before circulating through the rotor. For Cell 1, however, the LTST model showed a larger time delay compared to the rest of the cells. The difference can be related to the tracer injection location, because in Cell 1 the injection was made at the cell feed entrance, in the cell feed box, while for the rest of the cells the tracer injection was made inside the cell, near the feed entrance, due to direct access constraints. Thus, the difference is that the fresh feed entering the cell from the feed box was preferentially circulated to the rotor through the false bottom and the draft tube, while the tracer injected inside the cell was partially mixed with the internal circulating load and part of this flow was directly addressed to the tails.

RTD of the rougher flotation bank. Figure 8 shows that the increase of the number of cells in the bank reduces the pulp short-circuit in the bank as well as the fraction of pulp that stay inside the cell for a longer time. Thus, it can be clearly observed how the mixing decreases (less RTD dispersion) by increasing the number of cells in an industrial flotation bank.

Also, Fig. 8 shows the good fit of the dimensionless LTST model Eq. (6) for Cell 1, as well as the good fit of the dimensionless N tank-in-series model, Eq. (2), to describe the RTD for banks of three, five and seven cells.

Table 3 shows the fitted parameters using the N cells model, Eq. (2), to describe the mixing condition in the bank of cells. Here, for the first cell of the bank, it was shown that the number N of equivalent perfect mixers was 1.5, otherwise the operation of a single cell was quite different from a perfect mixer (N = 1). However, for a bank of three or more cells, the number N of equivalent perfect mixer cells was closer to the actual number of cells in the flotation bank. This finding agrees well with previous results obtained in banks of smaller size cells (Yianatos et al., 2005a).

In addition, Table 3 and Fig. 8 show that the LTST model gave a better fit (lower error) than the N cells model for Cell 1, while for banks of three or more cells, the error was similar in both models.

Therefore, it is possible to conclude that the LTST model is better than the N cells model to describe the hydrodynamic

Table 3 — Comparison of N perfect mixer cells and LTST models for banks of cells.

Model	Parameter	1 cell	3 cells	5 cells	7 cells
N cells	N	1.5	3.2	4.9	6.8
	τ, min [1]	3.79	10.50	17.83	25.44
	L, min	0.90	2.17	3.85	4.67
	Error x 10^{-7}	9.9405	0.9939	0.7428	2.0700
	τ_{total}, min	4.69	12.67	21.68	30.11
LTST	τ_S, min	0.66	0.17	0.57	0.49
	τ_L, min	3.41	3.47	3.53	3.63
	L, min	0.79	1.91	1.08	1.17
	Error x 10^{-7}	1.5619	0.8873	0.8497	2.1590
	τ_{total}, min	4.86	12.83	21.58	30.01
Number of points:		4,150	4,450	4,150	4,450

[1] Mixing time for N cells.

Table 4 — Model parameters for 130- and 250-m^3

		Cell	
Model	Parameter	130 m^3	250 m^3
N cells	N	1.41	1.40
	τ, min [1]	4.33	5.51
	L, min	1.24	1.04
	Error x 10^{-6}	2.0862	2.0754
	τ_{total}, min	6.98	6.55
LTST	τ_S, min	0.60	0.76
	τ_L, min	4.08	5.19
	L, min	1.13	0.89
	Error x 10^{-6}	0.4159	0.3414
	τ_{total}, min	5.80	6.84
Number of points:		1,285	1,497

[1] Mixing time for N cells.

behavior of one single cell, but for banks of three or more cells, both models are good enough.

Dimensionless comparison of RTD of single mechanical cells of different size. Figure 9 shows the RTDs of single 130- and 250-m^3 mechanical cells, both experimental data and LTST model. A comparison of the RTDs shows that, despite one of the cells being nearly twice as large, the mixing conditions are quite similar, thus allowing for an effective scale-up in terms of the hydrodynamic behavior. RTD tests for the 250-m^3 cell were developed at the new installation of Minera Pelambres (Díaz, 2006). The LTST model showed an excellent fit to describe the hydrodynamic behavior of the 130- and 250-m^3 cells.

Table 4 is a summary of the model parameters. It can be seen that the number of perfect mixers found with the N cells model is similar for both cells (1.41 and 1.40), and the τ_L/τ_S ratio was also similar in both cells (6.8 and 6.9). Thus, it was verified that the LTST model was adequate for representing large flotation cells with nominal volumes of up to 250 m^3.

Comparison of the RTD of single mechanical cells and pneumatic columns. Figure 10 shows the dimensionless comparison of the mixing conditions in a single 130-m^3 mechanical flotation cell and in a 132-m^3 pneumatic flotation column (Yianatos et al., 2005b). Here, the liquid RTD shows that the column behaves closer to a perfect mixer if compared to the liquid RTD in the self-aerated flotation cell. This is due to the counter-current pulp/bubble swarm contact, at normal superficial air rates of 10 to 20 mm/s, and demonstrates that mixing and short-circuiting in industrial columns can be equal or larger than for large-size self-aerated mechanical flotation cells.

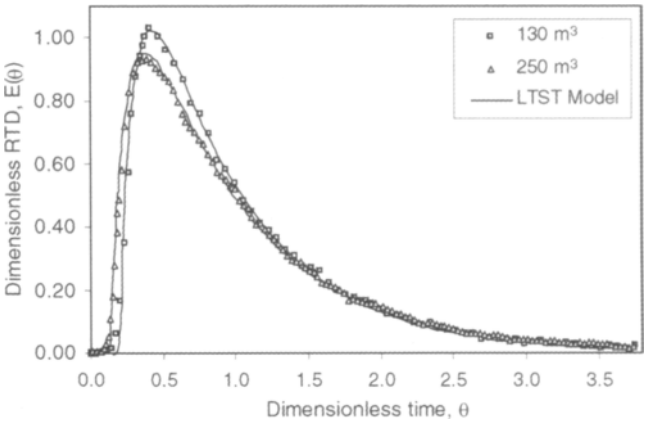

Figure 9 — Comparison of liquid RTD in 130- and 250-m^3 mechanical cells.

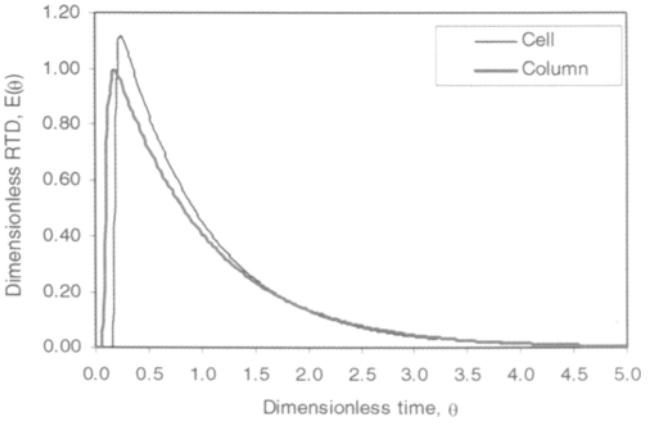

Figure 10 — Comparison of liquid RTD in a self-aerated mechanical cell vs. a pneumatic column.

Conclusions

The RTD of the 130-m^3 self-aerated flotation cells was evaluated, and it was confirmed that the flow regime was equivalent to more than one perfect mixer in series. This result is important to properly identify the collection rate constant in the industrial flotation process.

It was found that a large flotation cell could be better described by a simple LTST (large-and-small-tank-in-series) model with dead time, keeping the minimum number of parameters.

It was shown that the RTD of single mechanical cells is similar to that of large-size industrial flotation columns.

Comparison of 130 to 250 m^3 cells showed a similar dimensionless RTD. This result validates the use of the hydrodynamic pattern for scale-up purposes.

From a practical point of view, it was shown that the RTD of flotation banks consisting of three or more cells in series, i.e.,

for industrial flotation banks, can be well described considering the standard model of N perfectly mixed tanks-in-series plus a dead time, where N corresponds to the number of cells in the bank.

Acknowledgments

The authors are grateful to El Teniente Division Codelco-Chile for providing access to their plant and for valuable assistance in the experimental work. Funding for process modeling and control research is provided by CONICYT, project Fondecyt 1040100, and by Santa María University, project 270522.

References

Alexander, D.J., Franzidis, J-P., and Manlapig, E.V., 2003, "Froth recovery measurement in plant scale flotation cells," *Minerals Engineering*, Vol. 16, pp. 1197-1203.

Arbiter, N., 2000, "Development and scale-up of large flotation cells," *Mining Engineering*, Vol. 52, No. 3, pp. 28-33.

Bazin, C., and Hodouin, D., 1988, "Residence time distribution modelling for mineral process evaluation," *CIM Bulletin*, Vol. 81, No. 981, pp. 125

Bourke, P., 2002, "Selecting flotation cells: How many and what size?" MEI online, www.min-eng.com

Burgess, F.L., 1997, "OK-100 tank cell operation at Pasmisko-Broken Hill," *Minerals Engineering*, Vol. 10, No. 7, pp. 723-741.

Cortés, F.L., Yianatos, J.B., and Urtubia, H.C., 1995, "Characterization of the copper-moly collective flotation circuit at División Andina, Codelco-Chile," *Proceedings of the Copper'95*, Mineral Processing and Environment Conference, A. Casali, G. Dobby, M. Molina and W. Thoburn, eds., IIMCh-CIM-AIME, Santiago, Chile, Vol. II, pp. 37-51.

Díaz, F, 2004, "Determinación de la distribución de tiempos de residencia en celda de flotación de gran tamaño (250 m^3) en evaluación en Minera Pelambres," Chilean Commission of Nuclear Energy, Santiago, Chile, Project Report, Diciembre, 48 pp.

Deglon, D.A., 2003, "A novel attachment-detachment kinetic model," *Proceedings of the Strategic Conference, Flotation and Flocculation*, fundamentals to applications, J. Ralston, J. Miller and J. Rubio, eds., Snap Printing, Australia, pp. 109-116.

Harris, C.C., 1978, "Multiphase models of flotation machines behavior," *International Journal of Mineral Processing*, Vol. 5, pp. 107-129.

Huber-Panu, H., Ene-Danalache, E., and Cojocariu, D.G., 1976, "Mathematical models of batch and continuous flotation," *Flotation*, AIME, M.C. Fuerstenau, ed., New York, pp. 675-724.

Jowett, A., 1961, "Investigation of residence time of fluid in froth flotation cells," *British Chemical Engineering*, Vol. 6, pp. 254-258.

King, R.P., 2001, *Modeling and Simulation of Mineral Processing Systems*, Butterworth Heinemann.

Larenas, J., 2006, "Characterization of Big Size Flotation Cells," Master Thesis, Universidad Técnica Federico Santa María, Valparaíso, Chile.

Lelinski, D., Allen, J., Redden, L., and Weber, A., 2002, "Analysis of the residence time distribution in large flotation machines," *Minerals Engineering*, Vol. 15, pp. 499-505.

Mavros, P., 1992, "Mixing and hydrodynamics in flotation cells," *Innovations in Flotation Technology*, P. Mavros and K.A. Matis, eds., NATO ASI Series, Kluwer Academic Pub., London, pp. 211-234.

Mehrotra, S.P., and Saxena, A.K., 1983, "Effects of process variables on the residence time distribution of a solid in a continuously operated flotation cell," *International Journal of Mineral Processing*, Vol. 10, pp. 255-277.

Niemi, A.J., 1966, "A study of dynamic and control properties of industrial flotation processes," *Acta Polytecnica Scandinavian*, Vol. 48, pp. 1.

Niemi, A.J., 1995, Role of kinetics in modeling and control of flotation plants," *Powder Technology*, Vol. 82, pp. 69-77.

Pérez-Correa, R., González, G., Casali, A., Cipriano, A., Barrera, R., and Zavala, E., 1998, "Dynamic modelling and advanced multivariable control of conventional flotation circuits," *Minerals Engineering*, Vol. 11, No. 4, pp. 333-346.

Polat, M., and Chander, S., 2000, "First-order flotation kinetics models and methods for estimation of the true distribution of flotation rate constants," *International Journal of Mineral Processing*, Vol. 58, pp. 145-166.

Seaman, D.R., Franzidis, J-P., and Manlapig, E.V., 2004, "Bubble load measurement in the pulp zone of industrial flotation machines-a new device for determining the froth recovery of attached particles," *International Journal of Mineral Processing*, Vol. 74, pp. 1-13.

Van Deventer, J.S.J., Feng, D., and Burger, A.J., 2001, "The use of bubble loads to interpret transport phenomena at the pulp-froth interface in a flotation column," *Chemical Engineering Science*, Vol. 56, pp. 6313-6319.

Woodburn, E.T., and Loveday, B.K., 1965, "The effect of variable residence time on the performance of a flotation system," *Journal of the South African Institute of Mining and Metallurgy*, July, pp. 612-628.

Yianatos, J.B., Henríquez, F.H., and Oroz, A.G., 2005a, "Characterization of large size flotation cells," *Minerals Engineering*, Vol. 19, pp. 531-538.

Yianatos, J.B., Bergh, L.G., Díaz, F., and Rodriguez, J., 2005b, "Mixing characteristics of industrial flotation equipment," *Chemical Engineering Science*, Vol. 60, pp.2273-2282.

Yianatos, J.B., Bergh, L.G., Condori, P., and Aguilera, J., 2001, "Hydrodynamic and metallurgical characterization of industrial flotation banks for control purposes," *Minerals Engineering*, Vol.14, No. 9, pp. 1033-1046.

Yianatos J.B., Bergh, L.G., and Aguilera, J., 2000, "The effect of grinding on mill performance at División Salvador, Codelco-Chile," *Minerals Engineering*, Vol.13, No. 5, pp. 485-495.

Appendix A

LTST model solution

The analytical solution for the LTST model in the time domain, Eq. (5) above, can be derived from the process transfer functions in the Laplace domain, as shown in Fig. A1.

Here, $G_P(s)$ represents the transfer function of the dead time and $G_S(s)$ and $G_L(s)$ represent the transfer functions of the perfect mixers for the small and large residence time, respectively. These functions are defined in a standard way as follows

$$G_P(s) = e^{-Ls} \tag{A1}$$

$$G_S(s) = \frac{1}{(\tau_S s + 1)} \tag{A2}$$

$$G_L(s) = \frac{1}{(\tau_L s + 1)} \tag{A3}$$

The overall process transfer function is

$$G(s) = \frac{e^{-Ls}}{(\tau_S s + 1)(\tau_L s + 1)} \tag{A4}$$

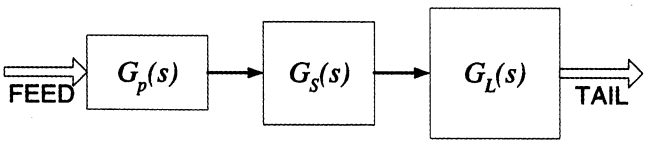

Figure A1 — Process transfer functions for LTST model.

Separating Eq. (A4) into partial fractions and rearranging gives

$$G(s) = \frac{e^{-Ls}}{(\tau_L - \tau_S)}\left[\frac{1}{\left(s + \frac{1}{\tau_L}\right)} - \frac{1}{\left(s + \frac{1}{\tau_S}\right)}\right] \tag{A5}$$

Then, taking the inverse Laplace transform from Eq. (A5) yields Eq. (5) in the main text.